

Dynamical consequences of CDM merger trees

Xavier Hernandez and William H. Lee

Instituto de Astronomía, Universidad Nacional Autónoma de México, Apdo. Postal 70–264, Cd. Universitaria, 04510 México D.F.

2 December 2024

ABSTRACT

Within the standard structure formation scenario, galaxies form as the result of an extended merger process. The first structures to form are small bound objects occurring at $z \sim 10$, which then merge repeatedly to form increasingly larger objects. In this context, elliptical galaxies are generally seen as the result of a major merger of spiral systems. Through extensive SPH simulations of merging spirals, we have explored these processes with the aim of quantifying their relaxation times. This is important, as it sets a minimum time interval between the onset of a merger, and the appearance of an elliptical galaxy. We then compare this constraint with predictions of the hierarchical scenario, computed through Press-Schechter merger trees. We find evidence for small elliptical systems which appear not to have been formed by a recent merger process.

Key words: galaxies: formation - galaxies: evolution - galaxies: elliptical and lenticular, cD - galaxies: interactions - cosmology: theory.

1 INTRODUCTION

In cosmology, the inflationary paradigm has not only provided an elegant answer to several disturbing problems of the standard Big Bang such as the horizon and the “flatness” problems, but also provides a mechanism for generating the primordial fluctuations from which we expect astrophysical structures to be formed. In most simple inflationary models, the initial spectrum of these fluctuations is a power law of the scale, and there is total absence of phase correlation among different scales. These properties lead to the hierarchical scenario of structure formation, where small scale objects merge continuously to produce increasingly larger ones as time goes by (e.g. White & Rees 1978; White et al. 1987).

The predictions of this model at large scale have been highly successful in matching the observed universe. N-body simulations of galactic clusters and super clusters match equivalent observed systems remarkably well. However, at galactic and sub-galactic scales considerable debate remains. Is the centrally concentrated dark matter density profile obtained from simulations of galactic dark haloes representative of the constant density cores seen in real galaxies or not (e.g. de Blok & McGaugh 1997; Firmani et al. 2001; Gnedin & Zhao 2002)? Is the level of substructure predicted by simulations at galactic levels compatible with the abundance of satellite systems in large galaxies, or are too many satellites being predicted (e.g. Moore et al. 1999; Ghigna et al. 2000)? Are the sizes of large disk galaxies compatible with the loss of angular momentum which models predict, mostly as a

consequence of the extensive merging regime these systems should have been subject to, which should probably have heated the disks beyond observed constraints (e.g. Navarro & Steinmetz 2000)?

It is clear that the assumptions going into the hierarchical model, at galactic and sub-galactic regions, remain subject to serious doubt. This is not surprising, since they result from large extrapolation of the direct analysis of primordial fluctuations performed at a much larger scale range, mostly through the study of the cosmic microwave background.

In this paper we shall examine another of the predictions of the hierarchical clustering scenario at the galactic level, namely the formation of elliptical galaxies through the merger of spiral systems. Through detailed Smooth Particle Hydrodynamics (SPH) simulations of the merger of two spirals, we will estimate the relaxation times for the process. Once this has been established, including a study of the variations expected given the extensive parameter space available to such a merger, and once the uncertainties in the initial conditions are considered, a consistency check for the theory is available.

Simulations of galactic mergers have been carried out many times before, but mostly aimed at obtaining very particular information, and rarely situated in a cosmological context, as what we attempt here. For example, Hibbard & Mihos (1995) explore merger remnant morphology and star formation, Barnes (2002) studies the formation of gas disks within merger remnants, Bendo & Barnes (2000) explore the distribution of line of sight velocities in merger remnants and remnant morphologies. We deemed it neces-

sary to repeat the experiment, paying particular attention to setting up the initial conditions in a cosmologically justified manner, as well as exploring the explicit dependence of the final relaxation times on the ample configuration parameter space.

Merger trees for large ellipticals can be constructed analytically, through the extended Press-Schechter formalism, and hence we have a prediction of the time elapsed between the last major merger and the present, for a galaxy of a given mass. This can be repeated, and given a redshift of observation, the hierarchical merger scenario predicts (on average) how far back in time the last major merger took place. This can be compared to the dynamical estimates of the relaxation time for the mergers. If the latter proves larger then the former, the theory needs revising.

In section (2) we describe the numerical scheme used to model a collision between spiral galaxies, as well as the different configurations tested. Section (3) gives the results of the different simulations, giving the relaxation time criterion we wanted to establish. In Section (4) we calculate the Press-Schechter merger trees for elliptical galaxies, and compare to the relaxation time criterion of the previous section. Finally, our conclusions are given in section (5).

2 MERGER SIMULATIONS

2.1 Numerical modeling

As stated in the introduction, we seek to obtain an estimate of the relaxation timescales for the merger of two spirals to result in a relaxed elliptical galaxy. Wanting to make a stringent comparison with models of structure evolution, we shall model the formation of a high redshift elliptical observed at $z \sim 1.0$. As we shall see, this implies starting the simulation at $z \sim 1.5$.

In attempting to model numerically the merger of two spiral galaxies, one must pay close attention to the gaseous component of the disk. It is this gas fraction through which most of the dissipation will take place, the other two components, stars and dark matter, being non-collisional. We hence used the method known as Smooth Particle Hydrodynamics (SPH), developed by Lucy (1977) and Gingold & Monaghan (1977), see Monaghan (1992) for a review. SPH is a Lagrangian method ideally suited for complicated three-dimensional flows, and has been used in a variety of astrophysical applications. We have specifically used the public code GADGET, developed by Springel et al. (2001) for galactic and cosmological simulations. This code allows us to trace shock fronts and other hydrodynamical features of the gas with great accuracy, as well as including an efficient N-body routine, to follow the dynamics of the non-collisional components. Further the code is fully parallelized, allowing it to run on a large number of computers simultaneously, as was done in our case.

In setting up the spiral galaxies which are to collide, the first thing is to construct each galaxy in isolation. As mentioned above, we include three components, a dark matter halo, a stellar disk and a gaseous disk, co-planar to the stellar one. In some variants, a stellar bulge was also added.

For the dark matter halo of each galaxy we chose a King sphere (King 1966). This has the advantage of includ-

ing a fully self consistent distribution function, with the density profile being a solution to a Boltzmann and a Poisson equation. In this way we set up a “live” halo, which will respond to the formation of the disk in its centre and, as the galaxies approach, to tidal effects and all other dynamics of the merger. Although cosmological simulations (e.g. Navarro, Frenk & White 1996) result in dark matter halos which are much more centrally concentrated than King spheres, direct observations of Dwarf Irregulars and low surface brightness (LSB) galaxies seem to imply the existence of constant density cores in the centers of galactic dark matter halos (e.g. Burkert & Silk 1997; de Blok & McGaugh 1997), which are inconsistent with cosmological profiles, even taking into account possible expansions of the core due to efficient ejection of the central baryonic component (Gnedin & Zhao 2002). Further, Hernandez & Gilmore (1998) showed that King halos produce rotation curves which are capable of matching both LSB and Dwarf Irregular and normal high surface brightness (HSB) observed rotation curves. Hernandez, Avila-Reese & Firmani (2001) also find strong evidence of a large constant density core in the dark matter halo of the Milky Way, in comparing the results of cosmological simulations of Milky Way formation, to extensive Galactic rotation curve determinations. It hence appears reasonable to model our dark halos as King spheres. King halos are defined by 3 parameters: the total mass of the halo, the total potential energy, and a shape parameter (through its variation we can assess the sensitivity of our results to the degree of central concentration of the galactic halos taken).

We take each of the dark haloes as having a velocity dispersion $\sigma = 130 \text{ km s}^{-1}$. A central density of $\rho_0 = 0.02 \text{ M}_\odot \text{ pc}^{-3}$ was assumed, in consistency with current estimates of this quantity obtained over a range of galactic systems (e.g. Firmani et al. 2000, Shapiro & Ilev 2002, Dalcanton & Hogan 2001). We used a central potential in units of the velocity dispersion $\Phi_0/\sigma^2 = 8.0$, shown by Hernandez & Gilmore (1998) to result in optimal rotation curves, from LSB to HSB systems. We obtain a core radius $r_c = 11.8 \text{ kpc}$, a tidal radius $r_{tidal} = 68r_c$ (where the density vanishes) and a total mass $M_{halo} = 1.35 \times 10^{12} \text{ M}_\odot$. The halos were modeled out to 35 core radii, by which time 94% of the total mass of the halo has been included, and the dynamical times have become comparable to the Hubble time at $z = 1.5$.

For the stellar component we take a double exponential disk given by:

$$\rho(r, z) = \rho_*(0) \exp(-R/R_*) \exp(-|z|/z_*), \quad (1)$$

With the scale length, R_* fixed at 3.5 kpc, resulting in a λ parameter for the total galaxy of ~ 0.05 . The vertical velocity dispersion for the stars was initially adjusted to yield a constant scale height of $z_* = R_*/5$. The normalization for the stellar disk was determined using a mass Tully-Fisher relation having a slope of 3.5, and normalized to the Milky Way (e.g. Giovanelli et al. 1997). When changes in the mass were explored, the disk scale lengths were scaled with the square root of the total disk mass, (e.g. Dalcanton, Spergel & Summers 1996; Avila-Reese, Firmani & Hernandez 1998), and the total disk mass scaled to the rotation velocity in the flat regime through the above mentioned Tully-Fisher relation.

The gas is initially distributed in an exponential disk having the same scale height as the stars, and a scale length

equal to twice the stellar scale length, as normal spirals tend to show (e.g. Dalcanton et al. 1996). The normalization of the gas disk is fixed by requiring that $M_g = F \times M_\star$ i.e. that the total gas mass is F times the total stellar mass. Values of 0.3 and 0.5 were explored for this parameter, representing gas rich disks. Both the stars and gas are given a rotation velocity in the plane of the disk to balance the total gravitational inward pull, over which is added an isotropic velocity dispersion, as required by the vertical scale height criterion mentioned above.

GADGET uses an ideal gas equation of state, $P = \rho u(\gamma - 1)$, where u is the internal energy per unit mass, and ρ is the mass density. One can in principle introduce an atomic cooling law, and trace the detailed thermal evolution of the gas component. However, this results in catastrophic cooling and clumping of the gas. The above result is natural, when one considers that the energy content of gas in a galactic disk is heavily determined by the turbulent regime it is in. Once energy is found at the atomic thermal level, it is radiated away, for all practical purposes instantaneously. However, an extended “waiting phase” is implied by the large scale turbulence, which is also the phase into which much of the heating processes feed into. Supernova explosions deposit a large fraction of their energy into pushing and blowing the inter stellar medium around, rather than representing a coherent thermal heating mechanism (e.g. Mac Low & Ferrara 1999; Mori, Ferrara & Madau 2002).

With this in mind, one can try to model the turbulence, star formation, supernova explosions, and feedback mechanism between the above, to model the gaseous component of a galaxy. This not only very expensive computationally, but will probably also yield a wrong answer, given the lack of a detailed microphysics for star formation and turbulence. Theoretical models and direct observations of galactic disks suggest the existence of efficient feedback regulation mechanisms between star formation and turbulent dissipation, capable of maintaining the turbulent gas at the threshold for gravitational instability. Examples of the above can be found in Firmani, Hernandez & Gallagher (1996), Martin & Kennicutt (2001), and Silk (2001). In this sense, it appears reasonable to model the gas component of our galaxies through isothermal equations of state, assumed to be representative of the turbulent phase of the interstellar medium. Indeed, several authors have taken this approach in the modeling of gaseous components of galaxies (e.g. Barnes 2002; Athanassoula & Bureau 1999).

We have thus chosen to use an isothermal equation of state, $P = c_s^2 \rho$, where c_s is the sound speed. We incorporated the necessary changes to the code to make use of this, with $c_s = 20 \text{ km s}^{-1}$ for most runs, and exploring the changes of this value on our final results.

We are hence assuming that heating processes, mainly shocks and supernova explosions at all times and at all places, exactly balance heat losses through viscous and turbulent dissipation. The above is well justified in isolated disks, were the gas naturally oscillates around the threshold of gravitational instability. In the more dynamic case of interacting and merging galaxies, the assumption breaks down whenever dynamical times become shorter than the 10 Myrs typical of the lifetimes of massive stars. This in effect sets a time resolution for our simulations, below which the details of our modeled mergers are probably unreliable. However, as

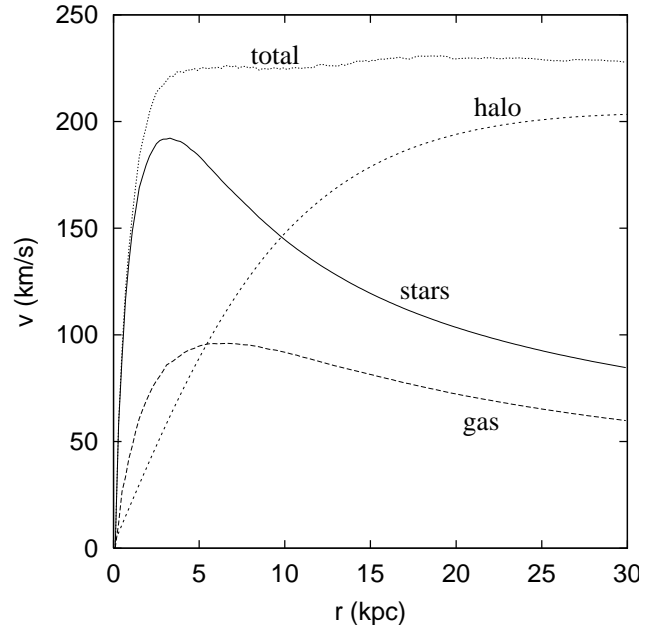


Figure 1. Rotation velocity curve, showing the total rotation curve as well as the contributions to this by the different components, in one of our modeled galaxies in isolation.

our main aim is to obtain the timescale for the completion of the merger, this detail becomes of little relevance.

2.2 Initial conditions

Each of the galaxies which are to collide is set up as indicated in the previous subsection, with the stellar and gaseous disks introduced inside the equilibrium dark halo. This allows the dark halo to adjust to the presence of the disks, and it reacts by increasing the concentration of the inner regions slightly.

Figure 1 shows the radial profile of one of our galactic models at the start of the simulation. The vertical axis gives the actual rotation velocity in km/s, shown by the thin dotted curve, and the contribution to it of the dark matter halo given by the thin dashed line. The contribution of the exponential stellar disk is given by the solid curve, and that of the gas by the thick dashed one. This is seen to match inferences for the Milky Way quite well, outwards of about 3.5 kpc, (e.g. Kuijken & Gilmore 1989; Wilkinson & Evans 1999). The inclusion of a stellar bulge component, would in fact yield a much better agreement. In any case, our modeled galaxy is seen to reproduce observed systems quite well in having soft core dark halos (e.g. Hernandez et al. 2001; de Blok, McGaugh & Rubin 2001; McGaugh, Rubin & de Blok 2001).

Once the disks are fully formed, the initial conditions for the dynamical evolution are established, and the merger is allowed to proceed. These initial conditions consist of a definition of the orbital plane for the encounter, an initial separation, an impact parameter, and the angular momentum vectors for the spins of the disks, defined in relation to the orbital plane.

The merger is clearly defined in a parameter space having several dimensions, the particular problem we are study-

ing limits some of these, the remaining we shall explore by varying the relevant parameters.

In comparing with Press-Schechter merger trees, we have to define the start of the merger as the moment when the two galactic halos form part of a single bound structure. In this sense, it will be when the centers of both galaxies are four virial radii apart. This is based on the result (Padmanabhan 1995) of the turnaround radius of a fluctuation being equal to twice the virial radius, at any redshift.

Hence initially the galaxies, together with their corresponding DM haloes, are placed at a distance $r_i = 4r_{virial}$, where r_{virial} is computed for a single galaxy from:

$$\frac{3}{4\pi r_{virial}^3} \int_0^{r_{virial}} \rho dV = 200\rho(z_1), \quad (2)$$

where $\rho(z_1) = \rho_0(1+z_1)^3$ is the critical density of the universe at redshift z_1 (a generic redshift at which the merger starts) and $\rho_0 = 3\Omega_M H_0^2/(8\pi G)$ is its present value. We take $z = 1.5$, $\Omega_M = 0.3$, $\Omega_\Lambda = 0.7$ and $H_0 = 65 \text{ km s}^{-1} \text{ Mpc}^{-1}$, a present standard set of numbers to define our cosmological scenario.

The above defines the initial separations, as a function of the galaxies used. If one of the galaxies is taken at a different mass, the initial separation is adjusted so that the dark halos start off touching each other, in terms of their turnaround radii.

The orbital plane is arbitrarily taken as the XY plane, with the galaxies staring off with zero radial relative velocities. We are assuming they have just detached from the Hubble expansion, and only as they begin to feel each other gravitationally will they develop an infall radial velocity. The tangential velocity is specified through the total λ parameter for the full system, where:

$$\lambda = \frac{L|E|^{1/2}}{GM^{5/2}} \quad (3)$$

Here L is the total angular momentum, W the potential energy of the system, and M the total mass. Given the cosmic distribution of λ parameters:

$$P(\lambda) = \frac{1}{\sigma_\lambda(2\pi)^{1/2}} \exp\left[\frac{-\ln^2(\lambda/\langle\lambda\rangle)}{2\sigma_\lambda^2}\right] \frac{d\lambda}{\lambda}, \quad (4)$$

with $\langle\lambda\rangle = 0.05$ and $\sigma_\lambda = 1.0$, (e.g. Dalcanton et al. (1996) and references therein), we expect the total system to have been spun up by the surrounding tidal fields much to the same degree as individual galaxies have. Most of the simulations were run with an orbital λ of 0.05, with one test at 0.025 being included.

The remaining degrees of freedom in setting up the merger are related to the orientation of the disks with respect to the orbital plane. We could perhaps expect both disks to co-rotate with the orbit, as each was spun up by a similar tidal field in the surroundings of the forming binary system. However, the large stochastic nature of the acquisition of angular momentum in galaxies (e.g. Catelan & Theuns 1996) suggests that one is probably well advised not to assume any *a priori* orientations. We have tested 6 different configurations, specified by the arrows in the second column of Table 1, where the orbital angular momentum is up.

All other initial conditions of the runs are also summarized in Table 1. Run C0 corresponds to a configuration

where the spin of both disks is aligned with the overall orbital motion. The orbital part of the dimensionless parameter λ is close to 0.05, as is that of all other runs, except for run C λ , which is close to 0.025. The deviations from these two numbers are due to the different orientation of the individual spins, which however make up only a fraction of the orbital angular momentum. In runs C0 to C5 we have changed only the relative orientations of the two disks, with respect to the orbital plane, with the following 10 runs being variations of run C0 with changes in impact parameter, disk scale radii of the galaxies, the presence of a bulge, the resolution of the simulation, the ratio of the masses of both systems, the gas fraction of the disks, the temperature of the gas disks, total mass of each galaxy and redshift at which the merger begins.

3 RESULTS

We now examine in detail a series of merger simulations, representative of the many cases we explored. Figure (2) gives temporal snapshots (vertical sequence) of the evolution of simulations C0, C1 and C3, on the first, second and third columns, respectively. The times on the horizontal rows are the same, in all cases 3.53, 4.12, 4.7 and 5.3 Gyr. The dots show the stellar component of both disks, and the line contours give projected gas density plots, with the much more extended dark halo particles not being shown. The physical scale is 300 kpc on each side.

The uppermost frame in Figure 2 shows the onset of the collision, the first 3.5 Gyr are spent by the disks in falling into each other, from the initial condition at $z = 1.5$. In case C0 both disks co-rotate with the orbital spin, and hence are seen face on, as all frames show the galaxies on the orbital plane. The third column also shows the galaxies face on, as in this case both disks are counter-rotating with the orbit, evolution up until the disks interact is hence identical to case C0. The central column shows a simulation in which one of the disks spins perpendicular to the orbital plane, which is seen clearly in its first frame, where one of them is seen edge on.

By the second row the first encounter has taken place, and both disks are seen at maximum separation after the initial impact. At this stage the morphology of the interacting systems is heavily dependent on the initial conditions, with the large angular momentum of the disks in simulation C0 giving rise to two well defined tidal tails, both in the gaseous component (line contours) and in the stars (dots). The large degree of incoherence in the angular momenta of the two disks in the other two simulations shown leads to a significant canceling of this component, and both gas and stars form two tight knots.

By the third row significant dissipation has taken place, especially in the gaseous component where strong shocks and tidally induced features develop. This now forms a dense bar in the central regions of the remnant, no longer characterized by the double nucleus morphology seen previously. A small tidal arm is seen in case C1, formed by gaseous and stellar material formerly associated to the co-rotating galaxy. By this time the differences between the three cases are beginning to fade. The final row shows the state of the remnants at the time when the temporal fluctuations

Table 1. Basic parameters for each run. The table lists for each run (labeled) the initial spin configuration, the angular momentum parameter λ , the redshift z for which the initial condition was constructed, the total mass of the system (in units of the mass of a single “standard” galaxy, used for run C0), the gas fraction with respect to stars, the mass ratio q , the speed of sound c_s , the scale radii for the stellar disks, the presence of a stellar bulge, and the total number of particles used in the simulation, $N = N_{\text{halo}} + N_{\text{star}} + N_{\text{gas}} + N_{\text{bulge}}$. In all cases $N_{\text{halo}} = 20,680$, $N_{\text{gas}} = N_{\text{star}} = 15,706$ and $N_{\text{bulge}} = 0$, except for run CN, where $N_{\text{gas}} = N_{\text{star}} = 31,732$, and run Cb, where $N_{\text{bulge}} = 15,706$.

Run	Spins	λ	z	M_t	$M_{\text{gas}}/M_{\text{stars}}$	q	$c_s(\text{km s}^{-1})$	$R_{\text{star}}(\text{kpc})$	Bulge	N
C0	$\uparrow\uparrow$	0.082	1.5	2.0	0.5	1.0	20.0	3.50	no	52,092
C1	$\uparrow\rightarrow$	0.069	1.5	2.0	0.5	1.0	20.0	3.50	no	52,092
C2	$\uparrow\downarrow$	0.055	1.5	2.0	0.5	1.0	20.0	3.50	no	52,092
C3	$\downarrow\downarrow$	0.028	1.5	2.0	0.5	1.0	20.0	3.50	no	52,092
C4	$\downarrow\rightarrow$	0.043	1.5	2.0	0.5	1.0	20.0	3.50	no	52,092
C5	$\rightarrow\rightarrow$	0.061	1.5	2.0	0.5	1.0	20.0	3.50	no	52,092
C λ	$\uparrow\uparrow$	0.060	1.5	2.0	0.5	1.0	20.0	3.50	no	52,092
CR	$\uparrow\uparrow$	0.069	1.5	2.0	0.5	1.0	3.50	1.75	no	52,092
Cb	$\uparrow\uparrow$	0.078	1.5	2.0	0.5	1.0	20.0	3.50	yes	67,798
CN	$\uparrow\uparrow$	0.082	1.5	2.0	0.5	1.0	20.0	3.50	no	84,144
Cq	$\uparrow\uparrow$	0.050	1.5	1.5	0.5	0.5	20.0	3.50	no	52,092
B	$\uparrow\uparrow$	0.078	1.5	2.0	0.3	1.0	20.0	3.50	no	52,092
Cc	$\uparrow\uparrow$	0.082	1.5	2.0	0.5	1.0	15.0	3.50	no	52,092
Cm	$\uparrow\uparrow$	0.083	1.5	1.0	0.5	1.0	20.0	3.50	no	52,092
Cmz	$\uparrow\uparrow$	0.075	2.5	1.0	0.5	1.0	20.0	3.50	no	52,092
Cz	$\uparrow\uparrow$	0.075	2.5	2.0	0.5	1.0	20.0	3.50	no	52,092

in both total potential energies, total kinetic energies and isophote geometry disappear, and a final stable configuration is found. It is important to note that the total time for this to happen is the same for the three cases shown.

Figure 3 is totally analogous to Figure 2, but shows the result of simulations C3, Cb and B, on the first, second and third columns, respectively. This explores the dependence of our results on yet another different orientation, both disks perpendicular to the orbital plane (C3). The other two examples use the relative orientation of case C0, but include the presence of a stellar bulge component in both galaxies, middle column, Cb, and a significantly different gas fraction of 0.3, in the third row, case B.

Again we see that the transition morphologies are highly sensitive to the initial conditions, with strong tidal arms developing in any component which co-rotates with the orbit, and falling rapidly towards the centre when this is not the case. However, the final relaxation times are again in excellent agreement with what was seen in the three cases shown in Figure 2, equilibrium configurations are attained by 5.3 Gyr in all cases. Other initial orientations listed in Table 1 give analogous results.

Although no explicit star formation has been introduced, in the interest of avoiding the introduction of free parameters pertaining to unknown physics, we do assume implicitly a certain degree of star formation, to justify the use of a constant gas temperature. Case Cc (where the speed of sound is $c_s = 15 \text{ km s}^{-1}$) explores the sensitivity of our results to the actual value used for the gas temperature, and although intermediary morphologies are slightly affected, total relaxation times are not. Case C λ was calculated to explore the effect of changing the impact parameter, in this case reduced by taking the orbital part of the λ parameter for the system at 0.025. Again, intermediary morphologies are affected, but not final relaxation times, as is the case with changes in gas and stellar disk scale radii (case CR) and mass ratio of the two galaxies (case Cq). Finally, case CN was a re-run of case C0, but at double the numerical resolu-

tion for the gas and stellar components. No differences were observed with respect to case C0, showing that our results are robust in respect to numerical effects.

The relaxation times we find are hence seen to be independent of the initial orientation of the disks, the details of the disk structure, and the physical conditions within them. This suggests that our final relaxation times are merely a dynamical result, expected to be a function only of the free-fall times at the initial conditions. This suggests a scaling of the total relaxation times with $(1 + z_1)^{-3/2}$. We included simulation Cz to test this hypothesis, a case totally analogous to C0, but set up at $z = 2.5$. The results confirmed the scaling we expected, as did cases Cm (half the total mass at $z = 1.5$) and Cmz (half the total mass at $z = 2.5$). This allows us to express the total relaxation times of cosmologically constructed spiral galactic mergers as:

$$\tau_R = \frac{21.1}{(1 + z_1)^{3/2}} \text{Gyr} \quad (5)$$

where z_1 is the redshift at which the merger begins.

Finally, Figure 4 gives the temporal evolution of both the total potential and total kinetic energies for simulations C0, C1, C3, C5 and Cb, the first five of the cases shown in figures (2) and (3). It can be seen that the details of the first maximum/minimum in the energies vary slightly from case to case, but that in all cases no temporal oscillations remain beyond 5.3 Gyr, the conservative value which we have taken for the total relaxation times. Indeed, the fluctuations in isophotal geometry also ended by 5.3 Gyr in all cases.

4 COMPARISON WITH HIERARCHICAL MERGER TREES

4.1 Analytical formulation of the problem

In the previous section the relaxation timescale of a merger has been established through dynamical simulations and cosmologically motivated starting conditions, as a function

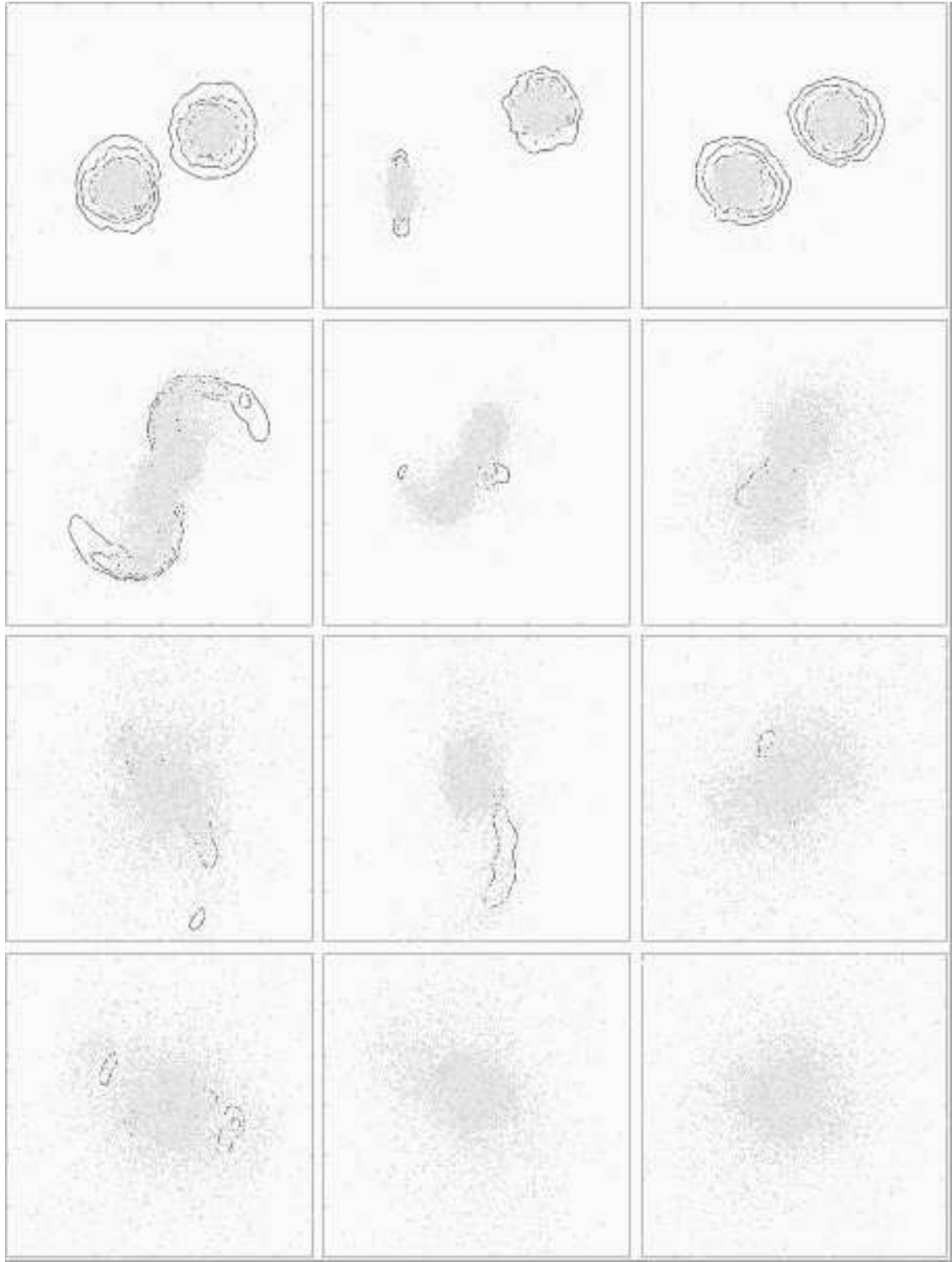


Figure 2. Snapshots of the dynamical evolution during the mergers for runs C0 (left), C1 (center) and C3 (right), in the orbital plane, at times $t = 3.53, 4.12, 4.7, 5.3$ Gyr from top to bottom. The contours are logarithmic projected densities and equally spaced every 0.5 dex, with the lowest one at $10^{-5} M_\odot \text{ pc}^{-3}$. The dots show the projected stellar particles. Each frame is 300 kpc on a side.

of the merger redshift. We now require an estimate of the formation timescale within the hierarchical clustering scenario. This will be done in a rigorous fashion by constructing merger trees within the extended Press-Schechter formalism, including all the cosmological details. However, before doing

this it is convenient to derive an approximate analytical solution, valid only in the simple $\Omega_M = 1, \Omega_\Lambda = 0.0$ scenario, and subject to numerous simplifying assumptions. This is done to obtain a clear understanding of the physics of the problem, and to provide an order of magnitude estimate to

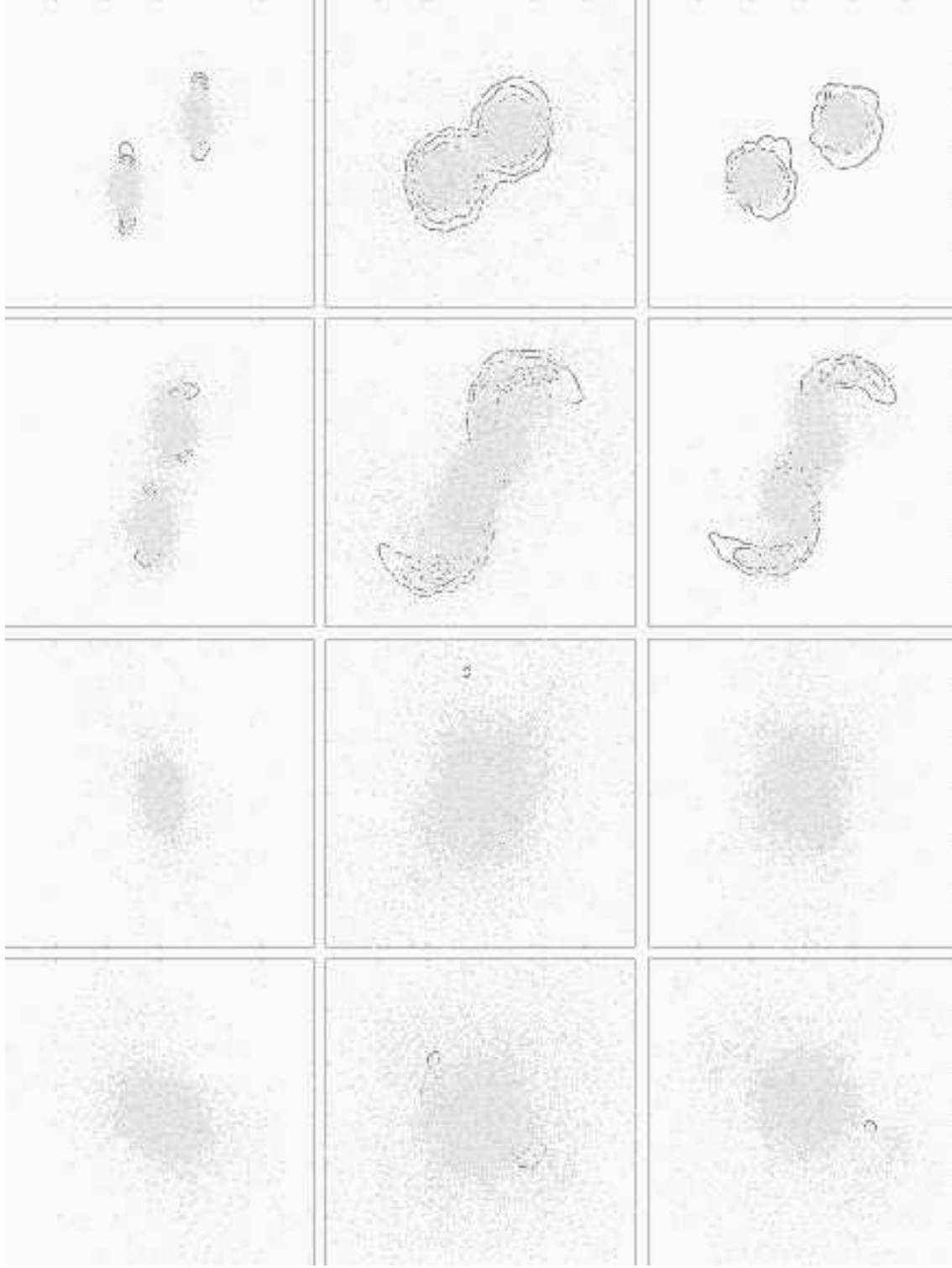


Figure 3. Snapshots of the dynamical evolution during the mergers for runs C5, Cb and B, in the orbital plane, at times $t = 3.53, 4.12, 14.7, 5.3$ Gyr from top to bottom. The contours are logarithmic projected densities and equally spaced every 0.5 dex, with the lowest one at $10^{-5} M_{\odot} \text{ pc}^{-3}$. The dots show the projected stellar particles. Each frame is 300kpc on a side.

the trends and values one should expect in the more rigorous numerical experiments.

The mass function of progenitors of an object existing at $z = z_0$ with mass M_0 , viewed at $z = z_1$ will be given by:

$$P(M_1) = \frac{M_0}{(2\pi)^{1/2}} \frac{\delta_c(z_1 - z_0)}{(S_1 - S_0)^{3/2}} \exp \left[\frac{\delta_c^2(z_1 - z_0)^2}{2(S_1 - S_0)} \right] \left| \frac{dS_1}{dM_1} \right| (6)$$

In the above equation $P(M_1)$ is the probability of finding a progenitor of mass M_1 , at $z = z_1$, where clearly $z_1 > z_0$

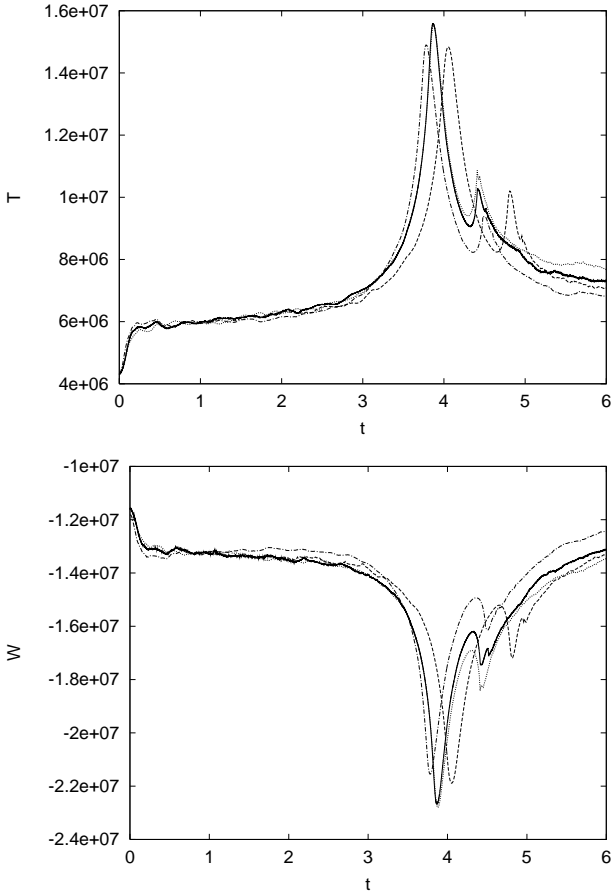


Figure 4. Kinetic (T) and potential (W) energies as a function of time for runs C0, C1, C3, C5, and Cb. Time is given in units of 9.8×10^8 yr, energies in units of 2×10^{53} erg.

(e.g. Lacey & Cole (1993); Nusser & Sheth (1999); Hernandez & Ferrara (2001)). $\sqrt{S_i}$ is the rms density fluctuation in a top hat window function of radius $(3M_i/4\pi\rho_0)^{1/3}$ and δ_c the critical over-density for collapse, with $\rho_0 = 3\Omega_M H_0^2/8\pi G$ being the present mean mass density of the universe.

As an example, figure(5) shows the mass function which results from having ‘factored out’ an observed object of mass $M = 10^{12} M_\odot$, $z_0 = 1.9$, amongst its progenitors at various higher redshifts, $z = z_1$. This figure was calculated within a full Λ CDM scenario, the results for a simplified cosmology being qualitatively identical. We see that as z_1 approaches z_0 , the mass function of progenitors tends to a delta function at $M_1 = M_0$, as was to be expected. At progressively higher redshifts, the mass functions are characterized by very well defined maxima, which shift to progressively lower masses (note the logarithmic scales on both axes). In this way, we see that for the above case, in going to redshifts higher than $z = 3.9$, the chance of finding a progenitor with a mass comparable to, say, $M_0/3$, sharply drops.

For the analytical calculation, we shall take a fixed $\delta_c = 1.7$ and $\Omega_M = 1.0$, as well as:

$$S(M_i) = S_8 M_i^{-1/3}, \quad (7)$$

valid for an effective spectral index in the galactic region of

$n = -2$, where S_8 is a normalizing factor to be fixed later (e.g. Padmanabhan (1995)).

The idea now is to identify the redshift z_{1Max} which corresponds to $dP(M_1)/dM_1 = 0$ evaluated at $M_1 = M_0/2$, as the redshift interval previous to z_0 , during which a major merger might have formed the object (M_0, z_0) , as further back in the past of this redshift, the chances of finding a progenitor having half the mass of the observed object drop abruptly.

Substituting the power law dependence for $S(M_i)$ in the rather cumbersome expression for $dP(M_1)/dM_1 = 0$, evaluated at $M_1 = M_0/2$ yields:

$$(z_1 - z_0) = \frac{1}{\delta_c} \left(\frac{S_8}{M_0^{1/3}} \right)^{1/2} \quad (8)$$

We can now evaluate S_8 from $S_8 M_8^{-1/3} = 1$, with:

$$M_8 = \frac{4\pi}{3} (8 \times 10^3 \text{kpc})^3 \rho_c, \quad (9)$$

yielding:

$$S_8 = 8 \times 10^4 \Omega_M^{1/3}. \quad (10)$$

i.e., a $\sigma_8 = 1$ normalization for the spectrum.

Substituting this last result, and the numerical value for δ_c into equation (8) yields,

$$\Delta z_M = 166 \left(\frac{\Omega_M}{M_0} \right)^{1/6} \quad (11)$$

The above expression gives the redshift interval, backwards of a redshift of observation, z_0 , beyond which it is unlikely that a major merger could have occurred, resulting in the observed object of mass M_0 , and defines the merger timescale. It is interesting that in the simplified cosmology taken for this calculation, no explicit dependence on z_0 remains.

Given that the initial conditions for the merger occurring at $z = z_1$ require that the two galaxies be placed at a separation of a multiple of their current virial radii, the relaxation timescale, τ_R will be estimated here as a multiple α of order unity of the free fall timescale for a system having 200 times the background density of the universe, hence,

$$\tau_R = \left(\frac{3\pi\alpha}{32} \right)^{1/2} \left(\frac{1}{200\rho_0 G} \right)^{1/2} (1 + z_1)^{-3/2} \quad (12)$$

Introducing numerical values, and using $t_H = (2/3)H_0^{-1}$ for the present age of the universe gives:

$$\tau_R = 0.17\alpha \frac{t_H}{(1 + z_1)^{3/2} \Omega_M^{1/2}} \quad (13)$$

Before comparing the above relation to the merger timescales of equation(11), we shall use:

$$1 + z_i = t_H^{2/3} t_i^{-2/3} \quad (14)$$

to arrive at:

$$166 \left(\frac{\Omega_M}{M_{Lim}(z_0)} \right)^{1/6} = (1 + z_0) \left[\left(1 + \frac{0.17\alpha}{\Omega_M^{1/2}} \right)^{2/3} - 1 \right], \quad (15)$$

for the mass $M_{Lim}(z_0)$ which at $z = z_0$ has a merger timescale equal to the relaxation timescale at the point at which the merger began. Introducing $\Omega_M = 0.3$ and $\alpha = 1.6$ yields:

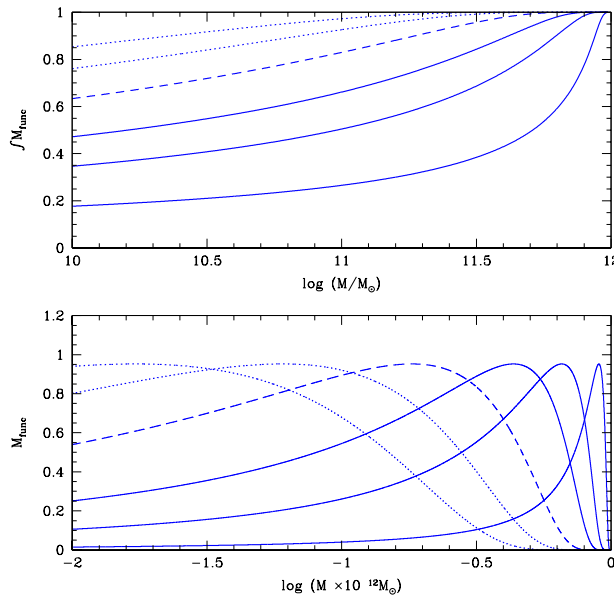


Figure 5. Lower panel: Mass functions of progenitors of a $10^{12} M_{\odot}$ system, observed at $z = 1.9$, at different previous redshifts: 2.4, 2.9 and 3.3, (solid curves), 3.9, (dashed curve), and 4.5 and 5.1 (dotted curves). All curves have been normalized to 1. **Upper panel:** Integral of the mass functions shown in the lower panel. It can be seen that for redshifts higher than 3.9 (dotted curves), the chances of obtaining one progenitor with a mass of $0.3 \times 10^{12} M_{\odot}$ or larger, drop below 5%, with the probability of two such fragments occurring being well below 0.25%.

$$M_{Lim}(z_0) = 6.4 \times 10^{15} (1 + z_0)^{-6}. \quad (16)$$

The above equation implies that at each redshift z_0 , there should be a maximum limit mass above which an observed system could not possibly look like a relaxed elliptical galaxy, as then the relaxation timescale becomes longer than the merger timescale, and the object should look like an interacting system. One can note that this holds even at $z = 0$, however, at a fairly large total mass of 6.4×10^{15} , which should be divided by a factor of about 20 to obtain stellar masses. Still, this limit mass is seen to fall very rapidly as $(1 + z_0)^{-6}$, and for example, for $M = 2 \times 10^{12}$ —in the range of estimates for the mass of our Galaxy (e.g. Wilkinson & Evans 1999; Hernandez et al. 2001)— we arrive at $z_0 = 2.8$ as the limit beyond which elliptical galaxies of that mass cannot be explained as having originated in a recent major merger. The choice of α was motivated by the results of the simulations performed here, and that of Ω_M by an attempt to come closer to a more realistic ΛCDM scenario. This last choice introduces a degree of inconsistency in the above calculation, which is only valid for $\Omega_M = 1$. However, as this is only intended as a conceptual guide, the result is probably a good first approximation.

4.2 Full ΛCDM comparisons

We shall now turn to more precise numerical calculations, the results of which can be understood more clearly by using the above results as a conceptual guide, and an order of magnitude estimate.

The lower panel of Figure 5 gives the mass functions of progenitors of an object of total mass $10^{12} M_{\odot}$, observed at $z_0 = 1.9$, at various higher redshifts $z_1 = 2.4, 2.9$ and 3.3 (solid curves), 3.9 (dashed curve), and 4.5 and 5.1 (dotted curves). This time the calculation was performed numerically evaluating equation (6) using a full ΛCDM scenario, with a fluctuation spectrum taken from Percival & Miller (1999). These curves are characterized by a maximum located at a value of the fragment mass which is a monotonically decreasing function of redshift. In this way, if the redshift at which the mass function of progenitors is calculated is close to the redshift of observation, the mass function becomes increasingly dominated by objects having a mass very close to that which the object has at $z = z_0$.

At redshifts much higher than the observation redshift, the mass function becomes dominated by progenitors having only a few hundredths of the mass of the observed object, e.g. the dotted curves for $z_1 = 4.5, 5.1$. It is clear that if we want to form the $10^{12} M_{\odot}$, observed at $z_0 = 1.9$ from a major merger, this cannot have taken place at such high redshifts. The solid curves show that this hypothetical major merger could well have taken place at a redshift of 2.4, 2.9 or 3.3, as at these values the mass function of progenitors for our $10^{12} M_{\odot}, z_0 = 1.9$ object includes a high probability of finding objects in the $(0.3 - 1.0) \times 10^{12} M_{\odot}$ range. This is clearly seen in the top panel, where curves corresponding to those of the bottom one give the integrals of the mass functions, normalized to 1.0, and hence the functions to be sampled if the progenitors of our test object are to be obtained, at any of the previous redshifts shown.

Although the mass functions at z_1 of 2.4, 2.9 or 3.3 do imply a high probability of finding progenitors in the “major merger” range, we cannot say that if the object $10^{12} M_{\odot}, z_0 = 1.9$ is an elliptical galaxy it was formed by a major merger having occurred in this redshift range. This is because in this redshift range, equation (5) implies that the relaxation timescale for such a merger, $\tau_R(z_1)$, is larger than the time intervals between any of those redshifts and $z_0 = 1.9$. This shows that if a major merger occurred between $z_1 = 1.9$ and $z_1 = 3.3$, the result at $z_0 = 1.9$ would be an interacting system, and not a relaxed elliptical galaxy. In fact, for this system, only just at the redshift $z_1 = 3.9$, corresponding to the dashed curve, does the relaxation timescale become equal to the time interval $z_0 - z_1$. This redshift $z_1 = 3.9$ also corresponds to the maximum redshift out to which there is some chance of obtaining a progenitor in the major merger range, defined as at least a 5% chance of obtaining one progenitor with a mass upwards of 0.3 times the mass at the observation redshift. This condition defines the merger timescale, Δt_M , which in this case is equal to τ_R .

In this way, we identify the observation redshift of mass of $z_0 = 1.9$ as the maximum redshift at which an elliptical galaxy of mass $10^{12} M_{\odot}$ can be observed, if it is to be thought of as having been formed by a major merger. Smaller redshifts at this mass result in cases where $\tau_R < \Delta t_M$, and hence suitable candidates for a major merger origin, if they are elliptical galaxies. On the other hand, larger redshifts at this mass satisfy the condition $\tau_R > \Delta t_M$, and would therefore look like interacting systems, if formed by a major merger.

We can now repeat the calculation, and look for the limit observation redshift, $z_{0lim}(M)$ above which the merger

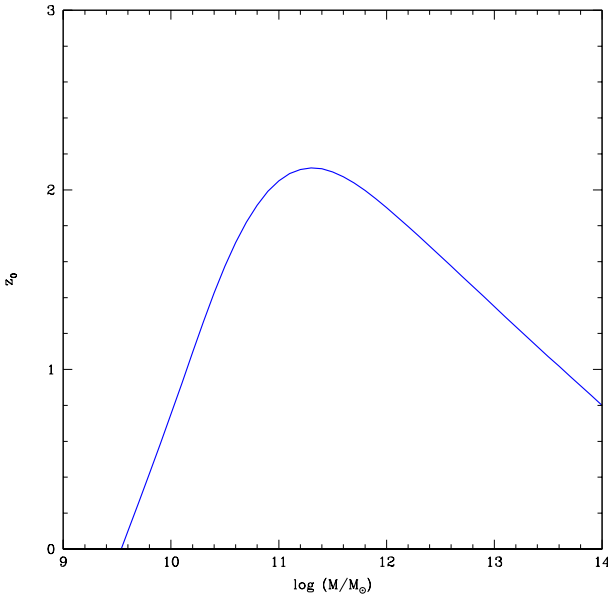


Figure 6. $z_{0lim}(M)$, the maximum observation redshift at which an elliptical galaxy of total mass M can be thought of as having been formed as the result of a recent major merger.

scenario fails for elliptical galaxies, as a function of total mass. This was done in constructing Figure 6, which shows $z_{0lim}(M)$, as a function of mass.

5 CONCLUSIONS AND DISCUSSION

In considering our results of Figure 6 we firstly note that the expected scaling obtained for the simple analytic case is found only at high masses, where the curve of $z_{0lim}(M)$ does indeed tend to a $M^{-1/6}$ scaling. However, the slight curvature found in the more realistic power spectrum, together with the high structure formation redshift in the Λ CDM scenario, result in a downturn at lower masses for this curve. This is interesting, as it establishes a maximum redshift of $z_0 = 2.1$ above which any observed elliptical galaxy, whatever its mass, falls above the $z_0 = z_{0lim}(M)$ curve, i.e. in the $\tau_R > \Delta t_M$ region. Any such elliptical galaxy would look like an interacting system, if it had formed as the result of a major merger.

Secondly we note that the region below the curve, where $\tau_R < \Delta t_M$, encompasses the majority of observed elliptical galaxies, which can hence be thought of as having been formed by the merger mechanism. However, the downturn at lower masses identifies a local maximum mass of $1.3 \times 10^{10} M_\odot$ ($6.3 \times 10^8 M_\odot$ in baryons), below which any observed ellipticals at any observation redshift $z_0 > 1.0$, must be thought of as having arisen through some mechanism distinct to the merger hypothesis. The corresponding limit at $z_0 = 0$ becomes $3 \times 10^9 M_\odot$ ($1.6 \times 10^8 M_\odot$ in baryons), comparable to the baryonic mass of may local dwarf ellipticals, larger than the few $\times 10^7 M_\odot$ in baryons inferred for the dwarf spheroidal satellites of the Milky Way.

This last point forms our strongest conclusion. There is direct observational evidence for the existence of ellipti-

cal galaxies for which the condition $\tau_R > \Delta t_M$ is met, and which within the hierarchical scenario of structure formation, in the observationally constrained Λ CDM scenario, should look like interacting systems, and not like relaxed elliptical galaxies at all.

A number of caveats might be suspected to apply to our study. It must be noted that we have used essentially present day galaxies and present day galactic scalings to model each of the spirals in the merger simulations. This is not entirely consistent, as our merger simulations take place at redshifts of 1.5 and 2.5. There is considerable evidence, both theoretical, within the framework of hierarchical structure formation models (e.g. Avila-Reese et al. 1998) and observational (e.g. Vogt 2001; Vogt & Phillips 2002) which implies very little or indeed no evolution of the mass Tully-Fisher relation with redshift. In this respect, the use of local values for this important structural relation for our high redshift galaxies is well justified.

The use of local disk scale length vs. disk mass relation however, is a different matter. Again both theoretical and observational studies of the redshift evolution of this scaling agree, giving a strong reduction in the disk scale length, in going to higher redshifts. This last point was not considered in the simulations, because including it would only lead to longer relaxation timescales, τ_R , and hence more dramatic, lower values of $z_{0lim}(M)$, at all masses. This is clear if one considers that in reducing the typical sizes of disks, one is limiting the action and effects of the tidal forces which bring about dissipation and relaxation in the merging galaxies, as these dynamical effects scale with the size of the objects upon which they act. In a limiting case, one can imagine very small and compact disks which could be treated as point masses, the ‘merger’ would not be more than the formation of a binary system in mutual orbit. Indeed, this effect starts to appear once the typical disk sizes become smaller than the distances of closest approach, relaxation times get longer and eventually tend to infinity, as the components become smaller. An analogous way of viewing this effect is to consider the typical density of the components. From a simplified classical tidal criterion, one can expect components to survive if their characteristic densities are higher than the average densities within their orbits.

The use of a centrally concentrated NFW profile would be demanded by consistency considerations in a hierarchical merger scenario. However, for the same reasons as those given above for the effect of reducing the disk scale lengths, the effect would also be to greatly extend relaxation times. In fact, given the divergent nature of cosmologically motivated dark halo density profiles, there will exist a pair of central regions which require very long times to lose their identities, and form a binary mutually orbiting system, with extended relaxation timescales.

It is hence clear that the use of local scaling laws and dark halos having constant density cores leads to a conservative estimate of $z_{0lim}(M)$, with results for a fully self consistent hierarchical scenario of structure formation yielding much more restrictive and lower values of $z_{0lim}(M)$, at all masses. The same can be said of the lack of a specific recipe for star formation, the introduction of which would result in the conversion of gas into stars i.e. of a dissipative component into a non-collisional ingredient, hence lengthening the relaxation times. This last effect would be enhanced in

the case of a starburst regime triggered by the pile up of gas in the central regions, and the subsequent loss of gas through a galactic wind, also increasing the fraction of the non-collisional stellar component.

Finally, we note that the arguments presented here are not the only objections that have been raised against the idea of all ellipticals being the result of major mergers. Wyse (1998) has pointed out that the high phase-space density seen in elliptical galaxies and early bulges is incompatible with the formation of these systems out of the dissipational merger of stellar disks. This last point can be alleviated by the introduction of a dissipational component, such as the gaseous disk, coupled gravitationally to the stellar component. However, the very red colours of elliptical galaxies at high redshift limits the amount of gas that can be included in such a merger, the details depending on the efficiency with which a galactic wind could subsequently clear the merger of gas. Mihos (2001) finds that ellipticals which fall into anomalous places in the central parameter relationship invariably appear as merger remnants, and concludes that if mergers are the formation mechanisms for elliptical galaxies, these must have taken place at very high redshift. Interacting and starburst systems seen at moderate redshifts cannot form a significant fraction of the local elliptical population.

There seems to be mounting evidence pointing to a high formation redshift for ellipticals, the results of our present study offering new support and being in accordance with the conclusions of a variety of independent studies centering on widely different aspects of the physics of the problem. It is perhaps time to consider what modifications are needed in the present galactic assemblage scenario in order to make it compatible with a high formation redshift for elliptical galaxies.

ACKNOWLEDGMENTS

The authors wish to thank T. Padmanabhan and C. Firmani for helpful discussion, and the Institute of Astronomy, Cambridge for its hospitality during the final phases of this work. Support for this work was provided by CONACyT (27987E) and (I39181-E) and DGAPA-UNAM (IN-110600).

REFERENCES

Athanassoula E., Bureau M., 1999, *ApJ*, 522, 699
 Avila-Reese V., Firmani C., Hernandez X., 1998, *ApJ*, 505, 37
 Barnes J. E., 2002, *MNRAS*, 333, 481
 Bendo G. J., Barnes J. E., 2000, *MNRAS*, 316, 315
 Burkert A., Silk J., 1997, *ApJ*, 488, 55
 Catelan P., Theuns T., 1996, *MNRAS*, 282, 455
 Dalcanton J. J., Hogan C. J., 2001, *ApJ*, 561, 35
 Dalcanton J. J., Spergel D. N., Summers F. J., 1996, *ApJ*, 482, 659
 de Blok W. J. G., McGaugh S. S., 1997, *MNRAS*, 290, 533
 de Blok W. J. G., McGaugh S. S., Rubin V. C., 2001, *AJ*, 122, 2396
 Firmani C., Hernandez X., Gallagher J., 1996, *A&A*, 308, 403
 Firmani C., D'Onghia E. D., Avila-Reese V., Chincarini G., Hernandez X., 2000, *MNRAS*, 315, L29
 Firmani C., D'Onghia E. D., Chincarini G., Hernandez X., Avila-Reese V., 2001, *MNRAS*, 321, 713
 Ghigna S., Moore B., Governato F., Lake G., Quinn T., Stadel J., 2000, *ApJ*, 544, 616
 Gingold R. A., Monaghan J. J., 1977, *MNRAS*, 181, 375
 Giovanelli R., Haynes M. P., Herter T., Vogt N. P. 1997, *AJ*, 113, 22
 Gnedin O. Y., Zhao H., 2002, *MNRAS*, 333, 299
 Hernandez X., Avila-Reese V., Firmani C., 2001, *MNRAS*, 327, 329
 Hernandez X., Ferrara A., 2001, *MNRAS*, 324, 484
 Hernandez X., Gilmore G., 1998, *MNRAS*, 294, 595
 Hibbard J., Mihos C., 1995, *AJ*, 110, 140
 King I. R., 1966, *AJ*, 71, 64
 Kuijken K., Gilmore G., 1989, *MNRAS*, 239, 571
 Lacey C., Cole S., 1993, *MNRAS*, 262, 627
 Lucy L. B., 1977, *AJ*, 82, 1013
 Mac Low M., Ferrara A., 1999, *ApJ*, 513, 142
 Martin C. L., Kennicutt R. C., 2001, *ApJ*, 555, 301
 McGaugh, S. S., Rubin, V. C., de Blok, W. J. G. 2001, *AJ*, 122, 2381
 Mihos C., 2001, *ASP Conf. Ser.* 240, 143
 Monaghan J. J., 1992, *ARA&A*, 30, 543
 Moore et al., 1999, *ApJ*, 524, 19
 Mori M., Ferrara A., Madau P., 2002, *ApJ*, 571, 40
 Navarro J., Frenk C., White S., 1996, *ApJ*, 462, 563
 Navarro J., Steinmetz M., 2000, *ApJ*, 538, 477
 Nusser A., Sheth R. K., 1999, *MNRAS*, 303, 179
 Padmanabhan T., 1995, *Structure Formation in the Universe*, Cambridge University Press, Cambridge
 Percival W., Miller L., 1999, *MNRAS*, 303, 179
 Shapiro P. R., Iliev I. T., 2002, *ApJ*, 565, L1
 Silk J., 2001, *MNRAS*, 324, 313
 Springel V., Yoshida N., White, S. D. M., 2001, *New Ast.*, 6, 79
 Vogt N. P., 2001, Deep Fields, ESO/ECF/STScI workshop, p.112
 Vogt N. P., Phillips A. C., 2002, *AAS*, 200 4008
 White S. D. M., Frenk C., Davis M., Efstathiou G., 1987, *ApJ*, 313, 505
 White S. D. M., Rees M. J., 1978, *MNRAS*, 183, 341
 Wilkinson M. I., Evans W., 1999, *MNRAS*, 310, 645
 Wyse R. F. G., 1998, *MNRAS*, 293, 429